nature ecology & evolution

Article

https://doi.org/10.1038/s41559-023-02145-2

Ghost admixture in eastern gorillas

Supplementary Material

1. New data generation and quality assessment

Six mountain gorilla samples from the Bwindi national park were obtained from deceased individuals as part of the Mountain Gorilla Veterinary Project. Katungi and Kahungye died as infants. Semehe, Nyamunwa, Nkuhene and Bwiruka died as adults. A male Mount Tshiaberimu individual, Mukokya, was sampled under anaesthetic, an intervention as part of a study on the long-term survivability of the small group of Mount Tshiaberimu gorillas (numbering six at the time of sampling). All these samples were imported into the UK in compliance with the legislation for endangered species (CITES).

DNA was extracted from these samples and sequenced on Illumina Hiseq X to 90Gb per sample using non-PCR libraries. After mapping, we performed quality controls and dropped the sample Nkuhene due to very low quality, with 80% of read duplicates and 2X average coverage. The rest of the samples performed similarly to previous mountain gorilla and eastern lowland gorilla samples included in this study.

2. Exploratory phylogenomic analyses

Numerous possible ghost introgression scenarios exist in the context of a two clade topology, such as that of the gorillas. To explore the demographic history of gorillas we performed initial exploratory phylogenomic analyses, f-statistics and the admixturegraphs method as implemented in admixtools2[71]. Briefly, we converted the genotypes of the autosomes after quality filtering (Methods) to the eigenstrat format, adding one *Pongo pygmaeus* individual (SRS396836) as an outgroup[7], and retaining only positions where more than 25 individuals had high-quality genotypes. We then calculated pairwise f2-statistics (blgsize=500000) for the four gorilla subspecies and the orangutan individual. Then, we used the find_graphs function to determine the best fitting graphs with an increasing number of admixture edges from 0 to 5 (Supplementary Fig. 1), defining the orangutan individual as outgroup. The best graph without admixture correctly separates the two gorilla species. The best graph with one admixture edge likely represents substructure in western lowland gorillas, although with an admixture proportion of 0%. Still, this graph fits significantly better (bootstrap p-value 0.0002) than the graph without admixture edges. Further edges increase complexity first in western, then also eastern gorillas, but do not significantly differ from less complex graphs (bootstrap p-value >0.05). We caution that with increasing complexity and in the absence of a hypothesis, the reliability of this method is limited, as discussed extensively by the authors of the method[71]. Furthermore, with the large space of possible graphs when involving many recent and ancestral populations, different graphs are inferred when repeating the inference[72]. We also explicitly tested a graph with ghost admixture into the ancestor of eastern gorillas (Supplementary Fig. 2). This graph provides a better fit than one without admixture edges (p=0.002), but worse than the best graph with one edge (p=0.002).

A more general constraint is that if there had been ghost admixture into any of the four terminal populations (mountain gorillas, eastern lowland gorillas, western lowlands gorillas, Cross River gorillas), these statistics could be informative, as asymmetries between the clades would be introduced. Still, these could be confounded by gene flow between the terminal clades. When explicitly testing such asymmetries D(EG, EG; WG, Orang) or D(WG,WG;EG,Orang), we find no such signature for the eastern gorilla populations, and a weak signature (z score <4) of allele sharing between either Cross River gorillas and eastern gorillas or western lowland gorillas and the outgroup, as shown below (Supplementary Table A).

pop1	pop2	pop3	pop4	f4 score	Z
MG	ELG	WLG	Orang	0.000002	0.07
MG	ELG	CRG	Orang	-0.00004	-1.5
WLG	CRG	MG	Orang	-0.00008	-2.33
WLG	CRG	ELG	Orang	-0.0001	-3.67

Supplementary Table A: f4-statistics of the population configuration f4(pop1,pop2;pop3,pop4), with corresponding z-scores.

As such, we focus on exploring possible ghost introgression events into the common ancestor of either eastern or western gorillas. These represent biologically plausible scenarios, which f4-statistics and the admixture graphs method are not able to detect. Instead, we can apply statistical methods developed to detect introgressed fragments in individual genomes from an unsampled or ‘ghost’ population (*S** and hmmix), see Methods. We note that these methods require an ingroup population, which experienced introgression and an outgroup population, which did not. Hence a scenario of ghost introgression into the common ancestor of all extant gorillas would be undetectable under current approaches.

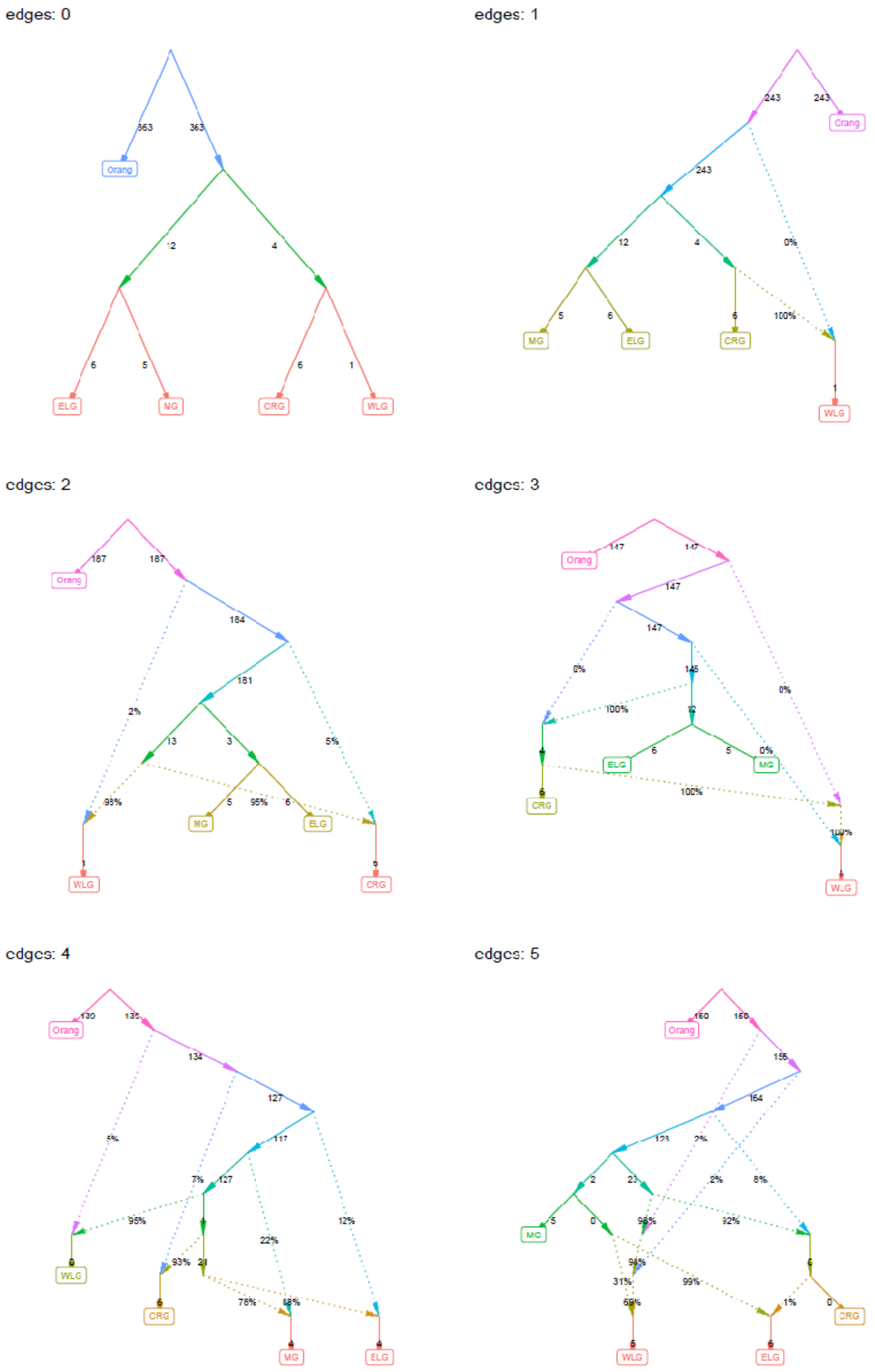

Supplementary Figure 1: Best fitting admixture graphs for up to five admixture edges for the four gorilla subspecies.

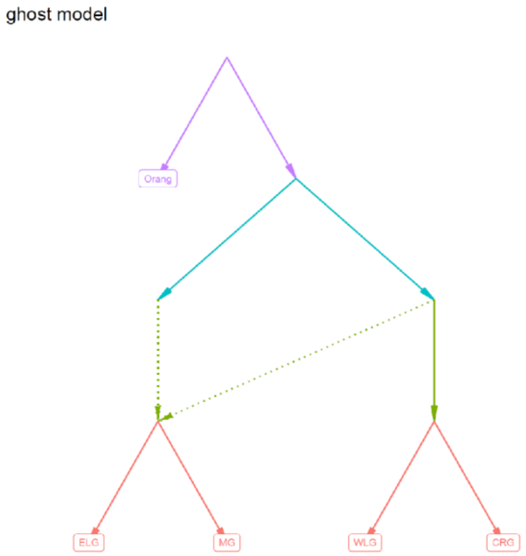

Supplementary Figure 2: Admixture graph with a ghost population contributing to the ancestor of eastern gorillas.

3. ABC modelling

The workflow of the main analyses regarding demographic modelling and putative introgressed fragments is shown in Extended Data Fig 1.

3.1 Initial demographic modelling based on the literature

Exploring the question of archaic introgression with the *S** statistic[19,20] requires a window-based demographic model, to test for outliers of the statistic. However, no previous demographic model had yet included all four known subspecies of gorilla. Moreover, due to the use of disparate data and methodologies previous demographic analyses of gorillas had resulted in widely divergent estimates for key parameters, including the estimated divergence time of the eastern and western gorilla species[9,13,14,28].

In an initial approach, we merged the parameters from the two most recent studies estimating gorilla demographic parameters, namely McManus et al.[13] and Xue et al.[8], see Supplementary Table 6. McManus et al.[13] applied a G-PhoCS approach to estimate current and ancestral population sizes, divergence times and gene flow between 9 western lowlands, 2 eastern lowlands and 1 Cross River gorilla in the model. We used parameters estimated by McManus et al.[13] under a human-gorilla divergence time of 12 mya, since this was the closest to the 13 mya human-gorilla divergence time more recently inferred by Besenbacher et al.[36]. Xue et al.[8] newly sequenced mountain gorillas from the Virunga subpopulation and inferred effective population sizes and divergence times from PSMC analysis.

We simulated this merged model in msprime[57] then in ms[55] in order to sample the mutation and recombination rates from a normal distribution and a negative binomial distribution respectively. We note that for the gorilla species split time we simulated using a 'low divergence' value of 261,000 years ago from McManus et al.[13], and a 'high divergence' value of 429,000 years ago estimated by Scally et al.[28] which is consistent with Mailund et al.[14]. The resulting distributions of segregating sites under both simulated models deviated substantially from those obtained using the empirical data (Supplementary Fig. 3). Under both models, we observe a similar, but larger number of segregating sites compared to the empirical data. As such we embarked on inferring a novel population-level demographic model for the extant gorillas using an ABC approach, as detailed in Methods. We note that both the McManus et al.[13] and Scally et al.[28] values for the gorilla species split time are substantially lower than that inferred in our ABC parameter inference at a weighted median posterior value of 965,481 years ago. Our estimate of a gorilla species divergence time is within the range of previous estimates, but at the upper end, for example Thalmann et al. similarly inferred a range of 0.9-1.6 mya[9]. Conceptually, a large divergence time is conservative for applying the *S** statistic, as the expected values increase with divergence time[22]. As such, we are conservative in our detection of putative introgressed fragments.

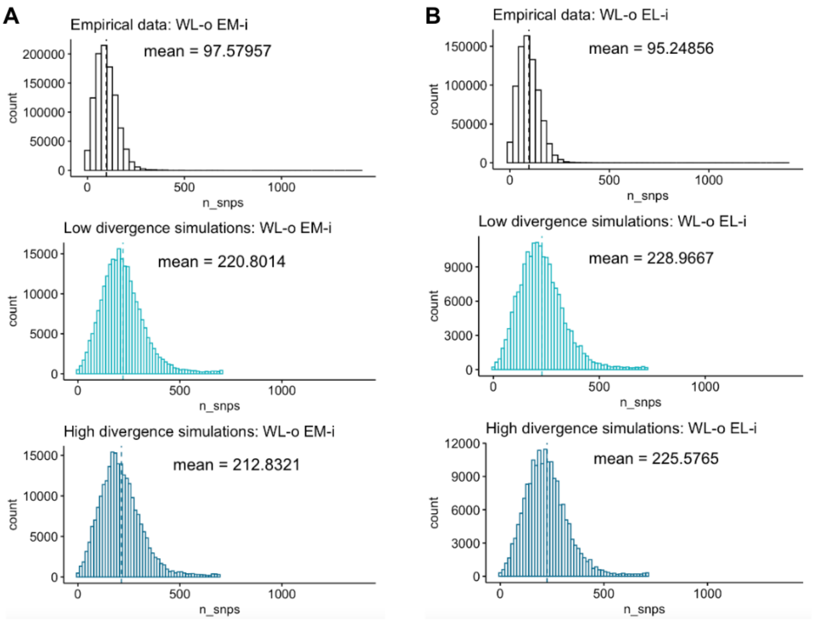

Supplementary Figure 3: Segregating site distributions in the empirical data, low divergence simulations and high divergence simulations under an initial merged model for **A** mountain gorillas and for **B** eastern lowland gorillas.

3.2 Summary statistic decorrelation

We assessed possible correlations between the summary statistics used in the ABC analysis. This could arise, as many of the summary statistics incorporated are related to the SFS. As such, we see substantial correlations between the highly related measures of fixed sites per individual, population-wise fixed sites and population-wise segregating sites (Supplementary Fig 4A). Correlated summary statistics in the ABC analysis could have two outcomes, it could introduce bias in the posteriors, or alternately, the redundancy simply captures the same information at the expense of adding additional statistics. In principle the neural network method we use to perform the ABC should be robust to any such correlations. Nonetheless we explored the impact of decorrelating the summary statistics on the posteriors obtained.

First, we simplified the correlated summary statistics using an *ad hoc* approach. We summed the correlated statistics (mean and standard deviations of fixed sites per individual, population-wise fixed sites and population-wise segregating sites), and used this one value as an input statistic, alongside the non-correlated statistics. Using this set of 'ad hoc' decorrelated summary statistics we performed the ABC analysis of parameter inference for the null model. The resulting posteriors did not differ greatly from those arising when using the correlated summary statistics as input.

Next we performed a formal decorrelation of the summary statistics. Wegmann et al.[73] recommend a partial least-squares (PLS) approach to obtain uncorrelated summary statistics. PLS aims to maximise the covariance between summary statistics and parameters in an approach which is conceptually similar to principal components analysis. Following [73] we applied a Box-Cox transformation on each summary statistic separately, to transform the data to be normally distributed. To perform the Box-Cox transformation and PLS analysis we followed the procedure detailed in the findPLS.R script provided by the ABCtoolbox package[74]. We performed a first pass of the PLS analysis defining 36 components, equal to the number of retained summary statistics after applying the Box-Cox transformation. The resulting root mean square error of prediction (RMSEP) plots indicated that the optimum number of PLS components was 10, which explained 95.6% of the variance (Supplementary Fig. 4B). As a confirmatory step we re-performed the PLS analysis with the optimum number of components (10) (Supplementary Fig 4C), following [75]. We then performed ABC parameter inference for the null model, using the 10 optimal PLS components as input for the summary statistics. We also performed ABC parameter inference for the subsequently 17 PLS components which explain 98.9% of the variance. In both cases the weighted median posteriors obtained were similar to those obtained using the original summary statistics (which include correlations). As such, we proceed with the original set of summary statistics for ABC analysis in the main text, but we introduce a logit transformation to ensure the posteriors would be within the distribution of the priors (Supplementary Fig 4D).

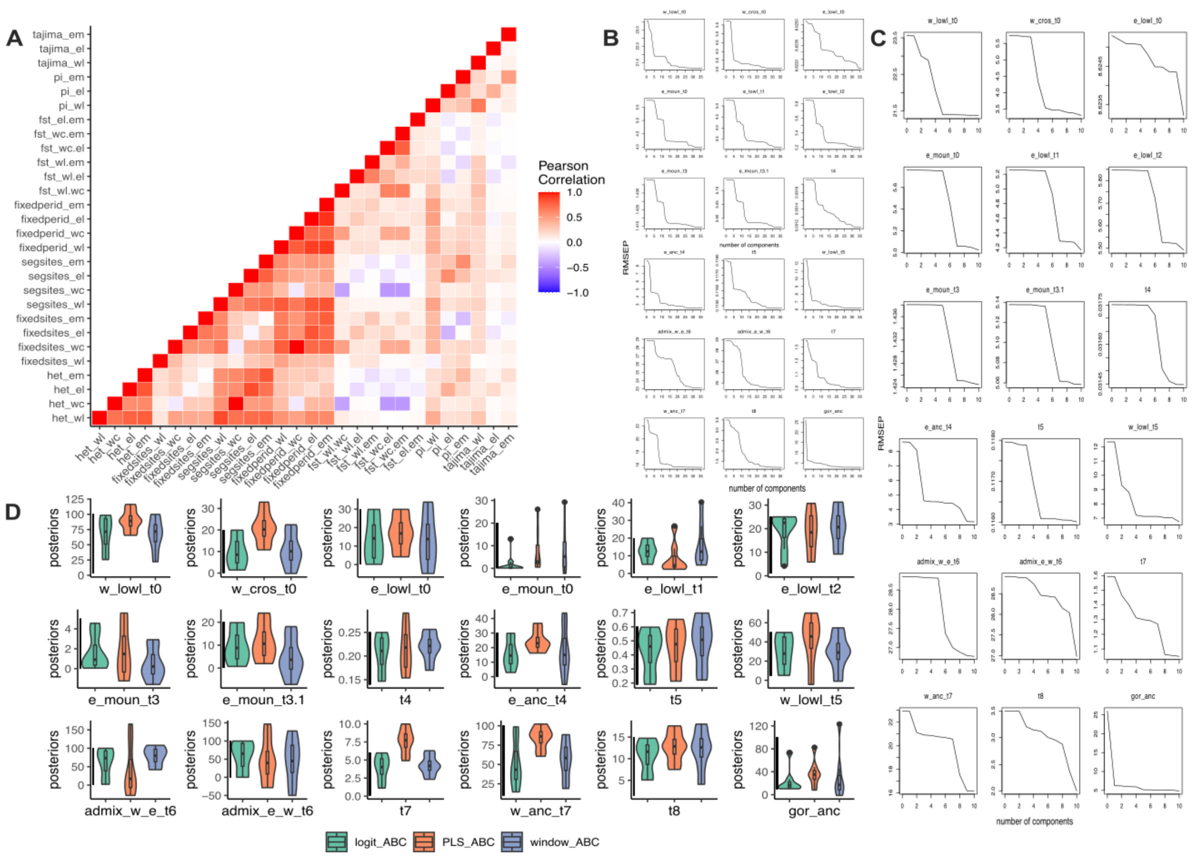

Supplementary Figure 4: A Summary statistic correlations. RMSEP plots with **B** 36 PLS components and with **C** the optimal 10 PLS components. **D** Posterior distributions under the final ABC protocol (teal, 'logit-ABC'), under the PLS-ABC protocol (red) which takes the 10 PLS components rather than the summary statistics as input and under the initial ABC protocol (purple) which used correlated summary statistics without a logit transformation. The black vertical line represents the prior distribution for each parameter. In panel D data are presented in violin plots with overlaid boxplots, which represent the median and interquartile range (25th and 75th percentiles). For the 3 models we generated n=35543 simulations, from which we accepted n=178 simulations under tol=0.005 for the final and initial ABC protocols and n=356 simulations under tol=0.01 for the PLS-ABC.

3.3 Adjusted demographic modelling

We inferred demographic parameters under a model without admixture from an unsampled lineage (Extended Data Fig 2A), as well as a model with such an admixture event into the ancestral western gorilla population (Extended Data Fig 2B), as described in Methods. We fixed parameters which were inferred well after inspecting the posterior distributions of the null model (with only the extant gorilla lineages) (Supplementary Fig. 5, Supplementary Table 2), and inferred a set of parameters including ghost admixture into the common ancestor of eastern (Extended Data Fig 3, Supplementary Table 2) or western (Supplementary Fig. 6, Supplementary Table 2) gorillas, respectively.

In the null model (without admixture from an unsampled lineage) we fix the parameters t1-t3 at the midpoint of their prior ranges, since these are very recent events, with narrow priors. In initial iterations of ABC-based modelling, we observed that parameters t1-t3 were contributing noise, but would contribute little information to the question of deeper demographic history, which is the main focus of the current study.

We also fix the parameter t6 (time of extant admixture between western lowland gorillas and the common eastern ancestor) at 34 kya. This was the result of converting continuous migration implemented by McManus et al.[13] to define migration pulses, using the midpoint between the western subspecies split time inferred by [13] and the present. All other parameters were allowed to vary in the null model, sampling from priors informed by previous literature (as detailed in Methods).

We provide a yaml file in the demes format[76], as drawn in Supplementary Fig. 7, for the best supported demographic model for gorillas, which includes a component of ghost admixture into the common ancestor of eastern gorillas.

We explored the impact of fixing well-inferred parameters from the null model on subsequent parameter inference in the ghost models in the section 3.4 Revised simulation approach.

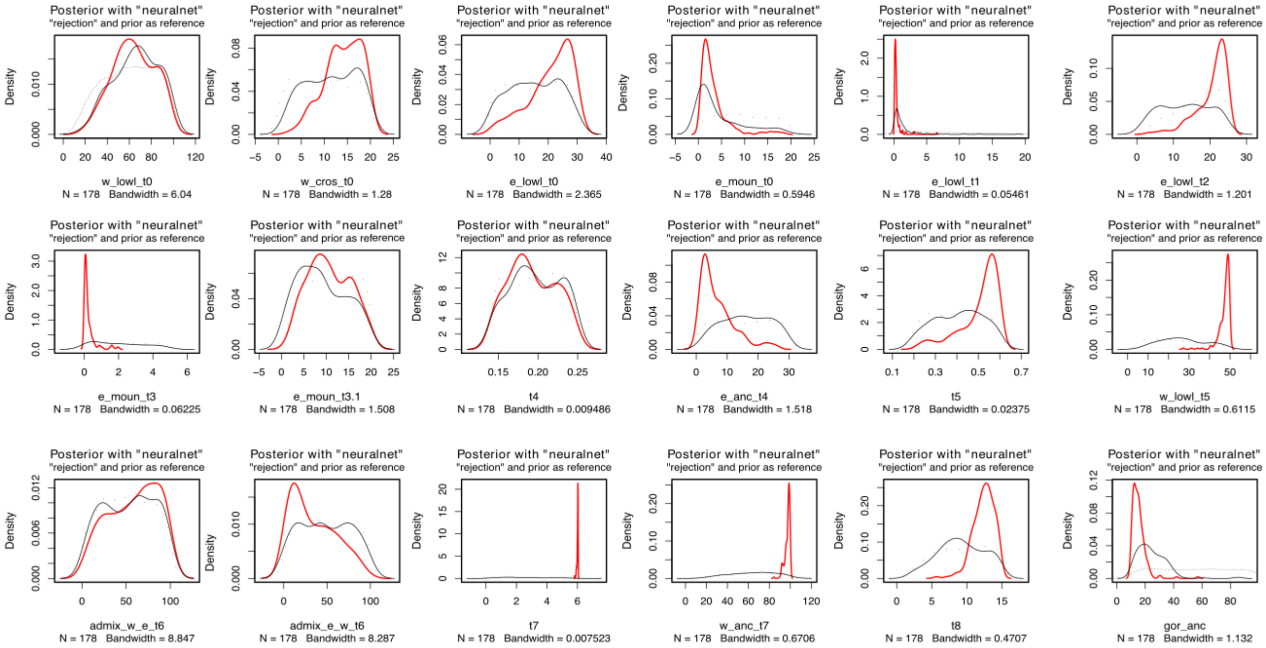

Supplementary Figure 5: Parameter distributions for all parameters inferred under the ABC null model. Red indicates the posterior distribution inferred with neural networks. Black indicates the posterior distribution inferred under a rejection method. The dotted grey line indicates the prior distribution.

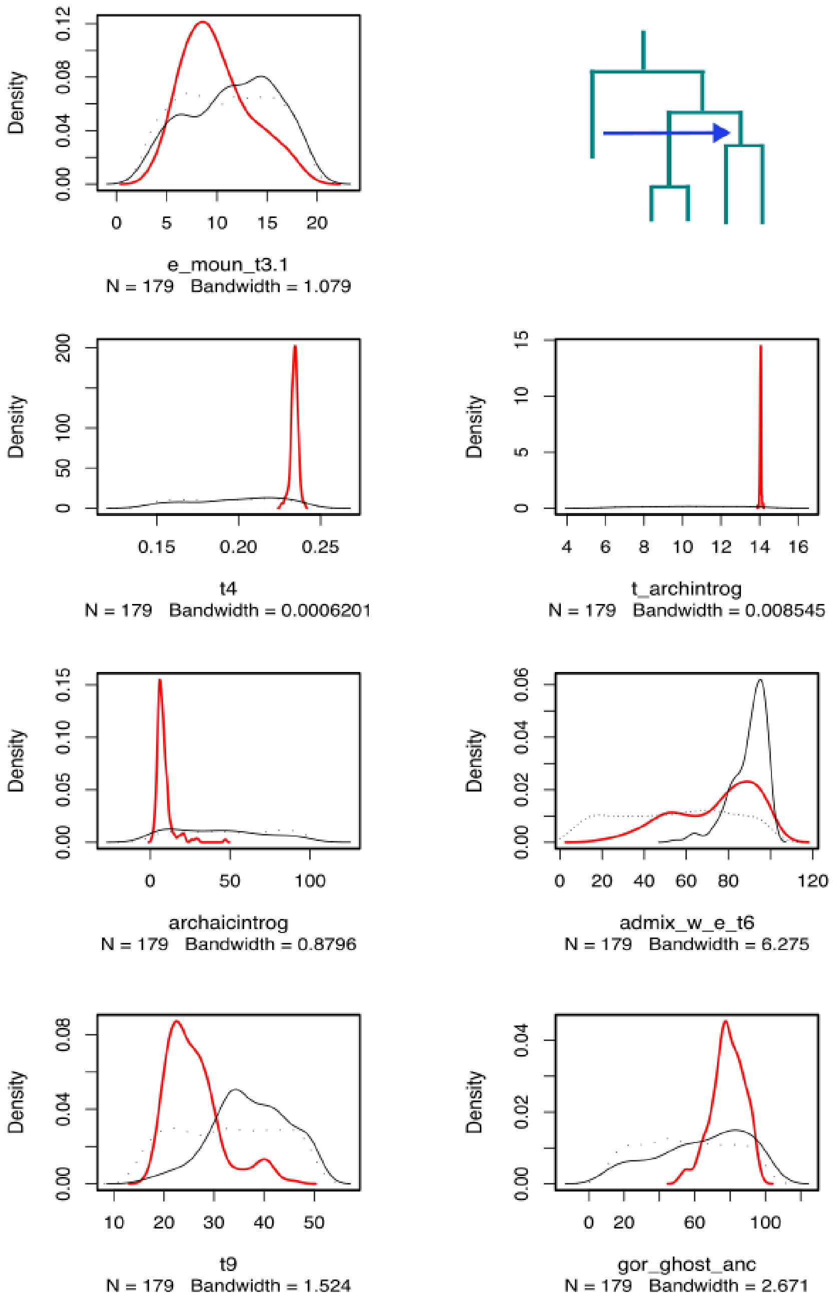

Supplementary Figure 6: Parameter distributions for all parameters inferred under the ABC model allowing gene flow from a ghost lineage into the common ancestor of western gorillas. Red indicates the posterior distribution inferred with neural networks. Black indicates the posterior distribution inferred under a rejection method. The dotted grey line indicates the prior distribution. We note under a model of ghost gene flow to the western common ancestor, the posteriors indicate a small contribution to the common ancestor of all gorillas (consistent with ancestral substructure), rather than a defined pulse to the western common ancestor.

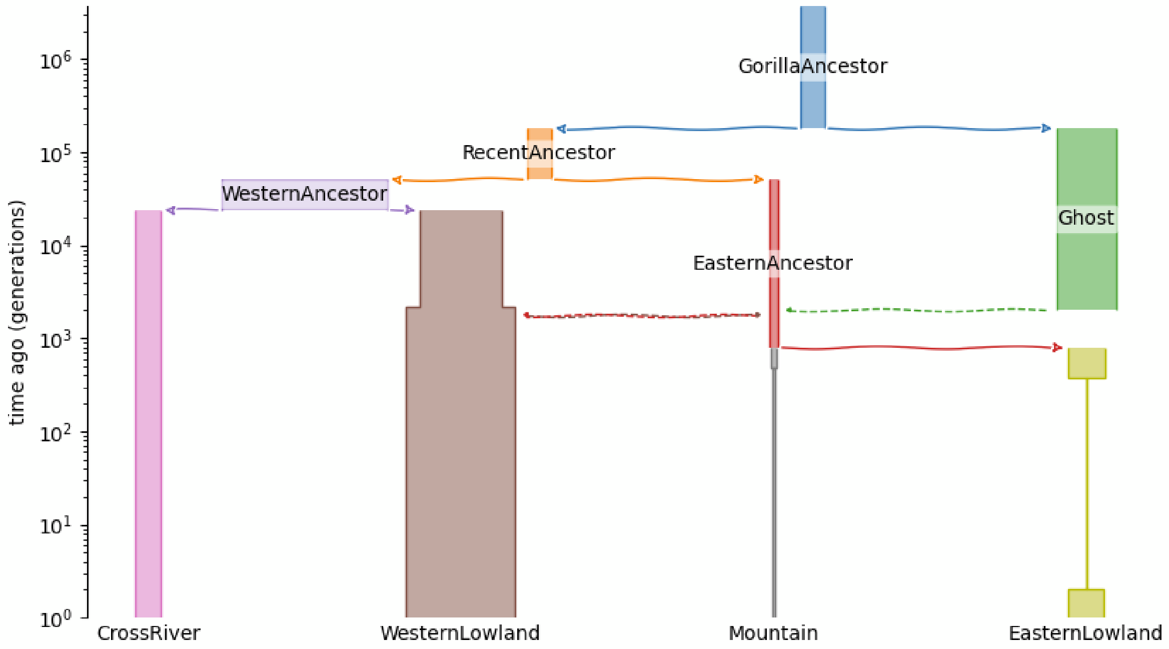

Supplementary Figure 7: Final demographic model with ghost admixture into eastern gorillas, implemented in demes (times in log-scale). The Python package demesdraw was used to generate this figure (https://github.com/grahamgower/demesdraw).

3.4 Revised demographic modelling

In our original ghost models, we fixed parameters with narrow CIs under the null model, in order to reduce the complexity of these models. To explore the ghost parameter space more fully we undertook a revised demographic inference approach for the ghost models, in which we sampled all parameters from priors (Supplementary Table 2). Again we allowed gene flow from a ghost lineage into the common ancestor of eastern gorillas or western gorillas respectively.

We note that sampling all parameters from priors considerably increases model complexity. Nonetheless, we obtain largely coherent results with those of our original ghost models (in which we fixed parameters well inferred under the null model), albeit with wider confidence intervals inferred (Supplementary Table 2, Supplementary Fig. 8-10).

Under the revised modelling, we infer 1.93% of ghost gene flow into the common ancestor of eastern gorillas, (0.33-2.45%, 95% CI) from a ghost population which diverged from extant gorillas ~3.1 Mya (1.43-3.77 Mya, 95% CI). We estimate the timing of ghost gene flow to have occurred 819 kya (146 kya-1.07Mya).

Whereas, for the revised model of ghost gene flow to the ancestral western population, the posterior distribution for the proportion of ghost gene flow tends to 0 (weighted median=0.43%; 0.01-1.98%, 95% CI), which is expected where there is no clear signal of introgression. Moreover, the timing of introgression in this scenario (weighted median=462 kya; 457-472 kya, 95% CI) tends towards the estimate for the extant gorilla species divergence time (weighted median=466 kya; 295-864 kya, 95% CI).

To compare the five demographic models A) null demography, B) original model of ghost gene flow into the eastern common ancestor, C) original model of ghost gene flow into the western common ancestor, D) revised model of ghost gene flow into the eastern common ancestor and E) revised model of ghost gene flow into the western common ancestor, we simulated 10,000 replicates of 250 windows of 40kbp length, fixing the parameters as the weighted median posteriors for each model. We calculated the posterior probabilities of each demographic model using the function postpr (tol=0.1, method="neuralnet"). Model B was overwhelmingly preferred, with the highest proportion of accepted simulations at 0.9988 and the highest Bayes factor at 823. In this model comparison, only simulations from models A and B were accepted. In cross-validation analysis the five models could be differentiated from each other (Supplementary Table 4).

We note that the weighted medians inferred under the original and revised demographic models for gene flow into the common ancestors of eastern and western gorillas respectively, are highly correlated, as expected (B and D: rho=0.8531903, p=1.075e-06; C and E rho=0.8870695, p=2.913e-06).

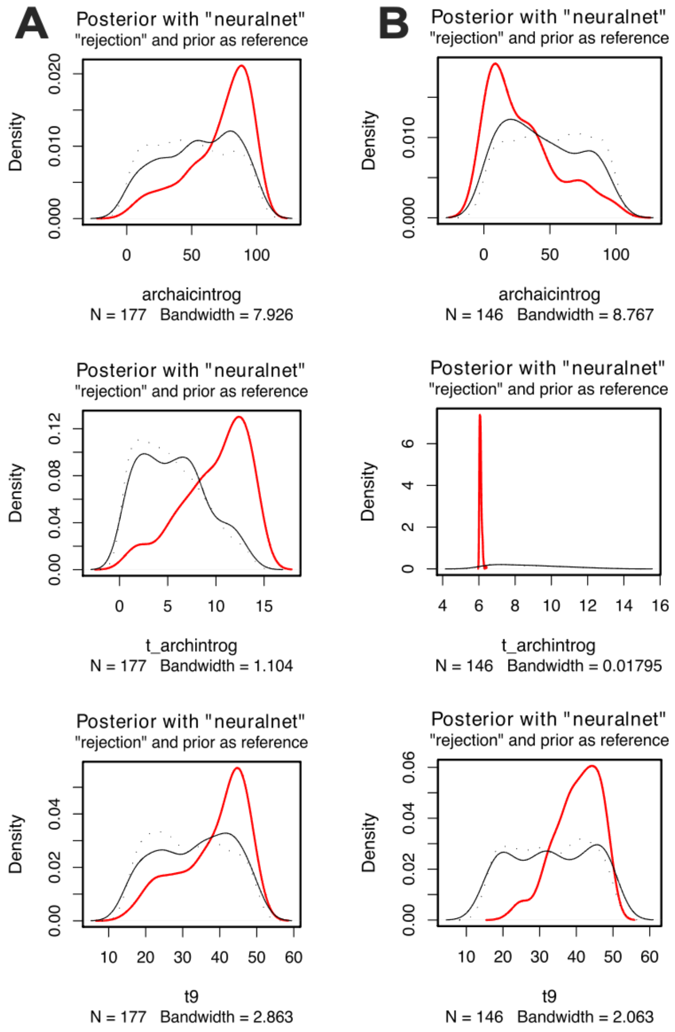

Supplementary Figure 8: Posterior distributions for the archaic introgression proportion, time of archaic introgression, and gorilla-ghost split time, for the revised models of ghost gene flow to **A** the common ancestor of eastern gorillas and **B** the common ancestor of western gorillas, sampling all parameters from priors. We note these are equivalent to Fig 2C, but for the revised ghost models (models D and E). The dotted line indicates the prior distribution. The black line indicates the posterior inferred with a simple ‘rejection’ algorithm. The red line represents the posterior inferred with neural networks. Distributions are plotted in ms units.

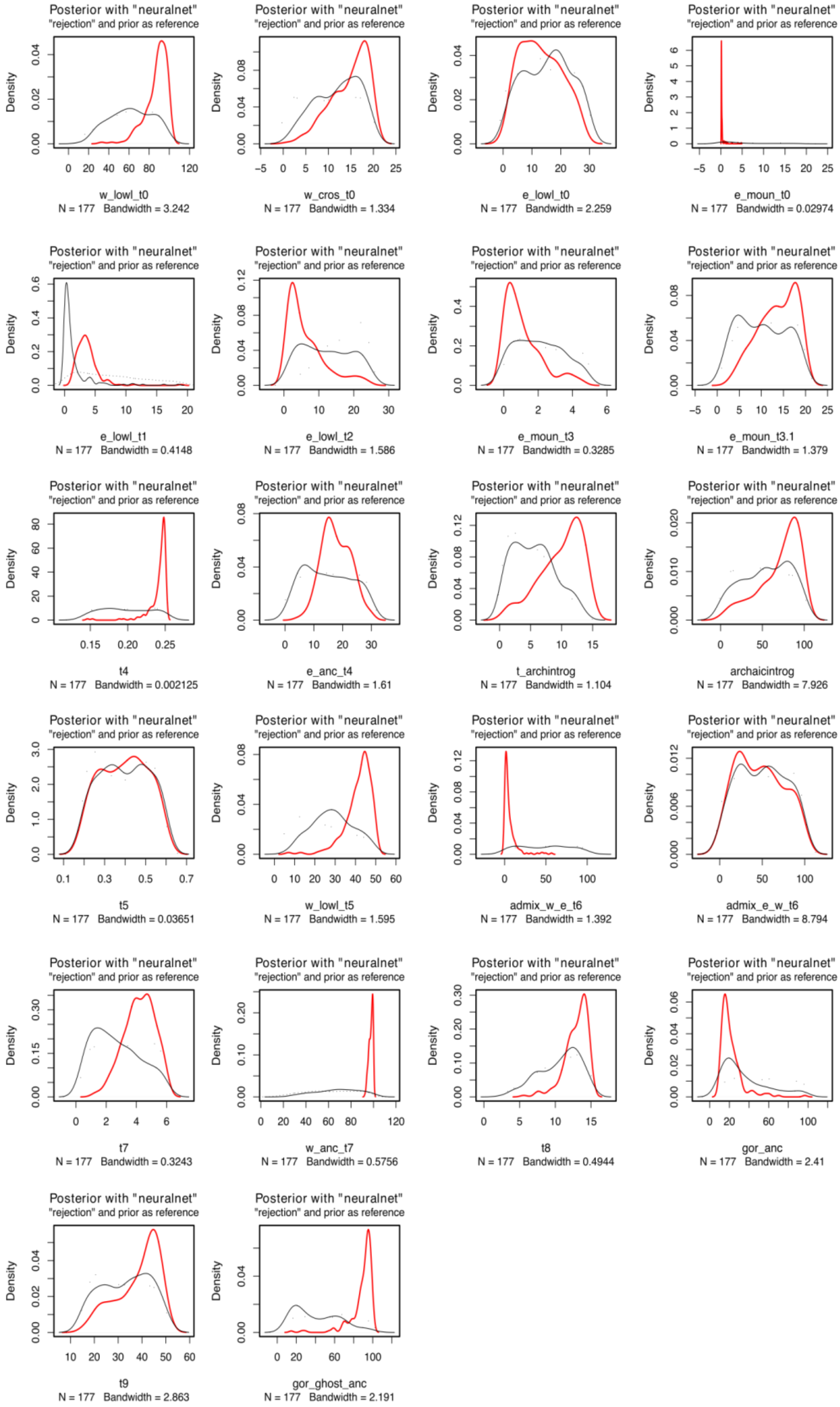

Supplementary Figure 9: Posterior distributions for all parameters inferred under the revised model of ghost gene flow to the common ancestor of eastern gorillas sampling all parameters from priors. Red indicates the posterior distribution inferred with neural networks. Black indicates the posterior distribution inferred under a rejection method. The dotted grey line indicates the prior distribution.

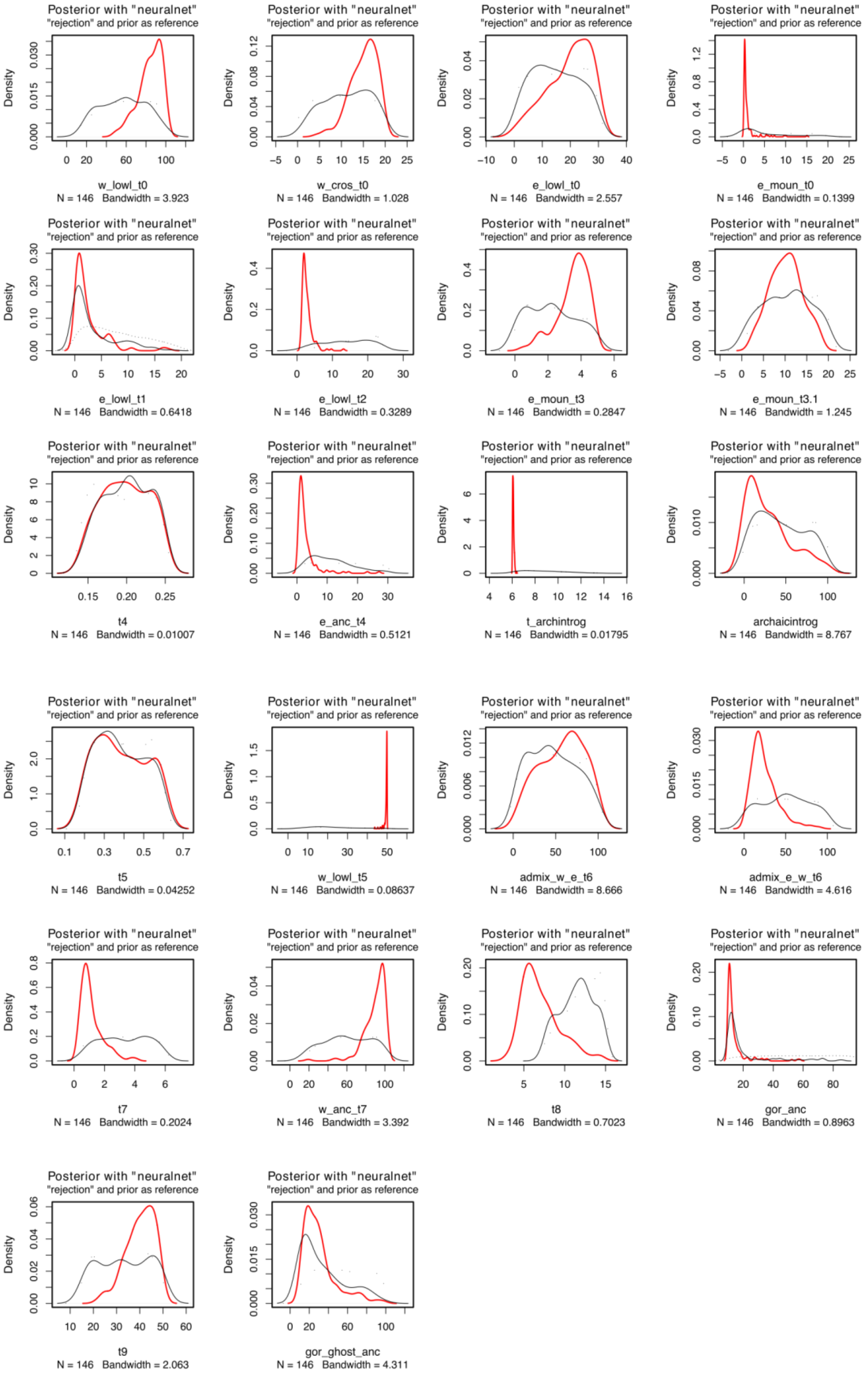

Supplementary Figure 10: Posterior distributions for all parameters inferred under the revised model of ghost gene flow to the common ancestor of western gorillas sampling all parameters from priors. Red indicates the posterior distribution inferred with neural networks. Black indicates the posterior distribution inferred under a rejection method. The dotted grey line indicates the prior distribution.

3.5 Parameters from hmmix

We inferred parameters from the HMM model in hmmix, as shown in Supplementary Table 10. The coalescence times between the two gorilla species are inferred at ~256 kya, which is more recent than the estimates from the ABC modelling. However, reversing ingroup and outgroup (i.e. using western lowland gorillas as potential ingroup and eastern gorillas as potential outgroup) yields a larger coalescence time of ~572 kya due to the larger effective population size. This relationship between population size and coalescence time makes it difficult to compare to the divergence times of the ABC modelling. Furthermore, we infer a coalescence time of gorilla and ghost segments in eastern gorillas at 1,520 Mya. However, the archaic percentage is inferred at 17.7%, which then represents a larger archaic proportion at a shallower coalescence. The calculated admixture time is ~69 kya, hence older than the one inferred in the demographic model as well. A thorough filtering for decoding the introgressed fragments with hmmix (Methods) leads to a largely overlapping set of candidate regions.

3.6 Validation of method performance

To assess the performance of the *S** statistic and hmmix and their robustness to demographic model misspecifications we performed validation analyses, following the approach of Huang et al.[29]. This is particularly pertinent for the *S** statistic, which requires a null demographic model (without ghost introgression) to determine outliers of the statistic.

We generated simulations using msprime[56,57] under different null demographic models and assessed the performance of the *S** statistic and hmmix using precision-recall curves (Extended Data Fig 4). We define precision as the number of true introgressed fragments of all introgressed fragments inferred, and recall as the number of inferred true introgressed fragments of all true introgressed fragments (ie recall represents the detection rate of true introgressed fragments) [29].

We simulated data and generated general linear models of the expected distribution of *S** scores under 1) the ABC-based null demographic model (Extended Data Fig 2A) which is the ‘main model’ here and 2) the ‘worst null model’, where we take the maximum value of the 95% credible interval for all ancestral Ne parameters (rather than the weighted median posteriors), this hence increases the number of highly divergent haplotypes present due to incomplete lineage sorting (ILS) (rather than introgression) (Supplementary Table 2).

We then simulated data under the model of archaic introgression into the eastern ancestor (model B), as well as a modified model of archaic introgression with the maximum values of the 95% credible interval for all ancestral Ne parameters (“worst” model B). We subsequently run *S** and hmmix, with a range of values for the quantile (threshold to define outliers of the statistic) of 0-0.999 for *S** and the posterior probability of 0-0.9999 for hmmix, following [29] (Supplementary Tables 7-8). For each model we simulated 200 Mb with 100 replicates and sampled 1 individual for the target population (eastern lowland or mountain gorillas) and 10 individuals for the outgroup population (western lowland gorillas).

Additionally, for the *S** statistic we explore a ‘worst mis-specified’ scenario, where we generate simulated data under the ‘worst model’ (with high ILS) but run the *S** analysis using the outlier values inferred for model A (expecting less ILS) (Extended Data Fig. 4).

4. Characterising introgressed fragments

4.1 General features

*S** scores are correlated with the numbers of segregating sites, as expected (Supplementary Fig. 11); putatively introgressed windows are observed for high *S** scores across this distribution, depending on the demographic model.

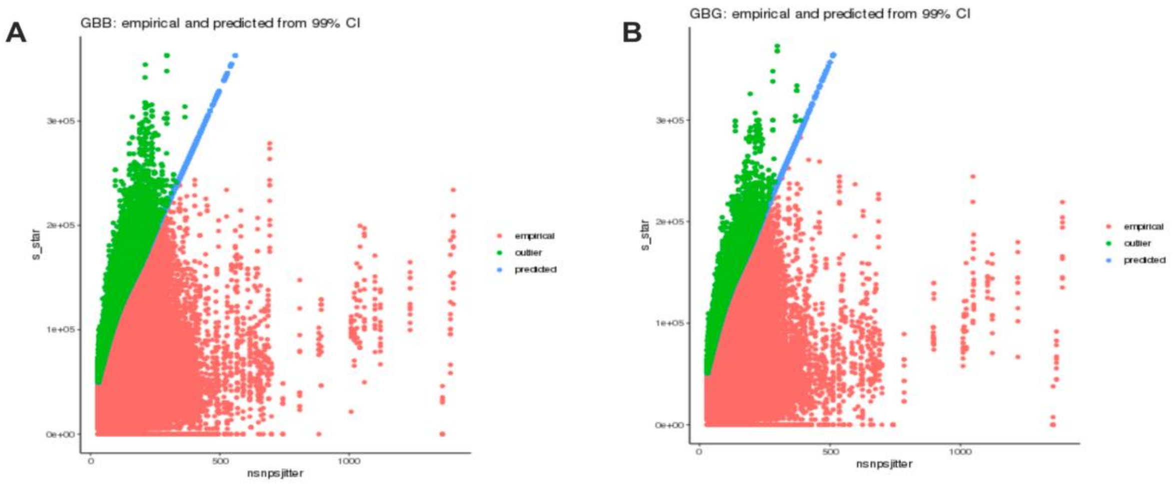

Supplementary Figure 11: Genome-wide distributions of *S** scores calculated in 40kb windows for **A** mountain gorillas as ingroup, western lowland gorillas as outgroup, **B** eastern lowland gorillas as ingroup, western lowland gorillas as outgroup. Red indicates the genome-wide distribution, blue the predicted *S** values under the general linear model (Methods) and green the outlier windows inferred under the 99% confidence interval.

We do not observe a significant difference in introgressed fragment length distributions between the eastern subspecies, as inferred under hmmix (p>0.01, Wilcoxon unpaired test for both 0.9 and 0.95 threshold) (Supplementary Fig 12).

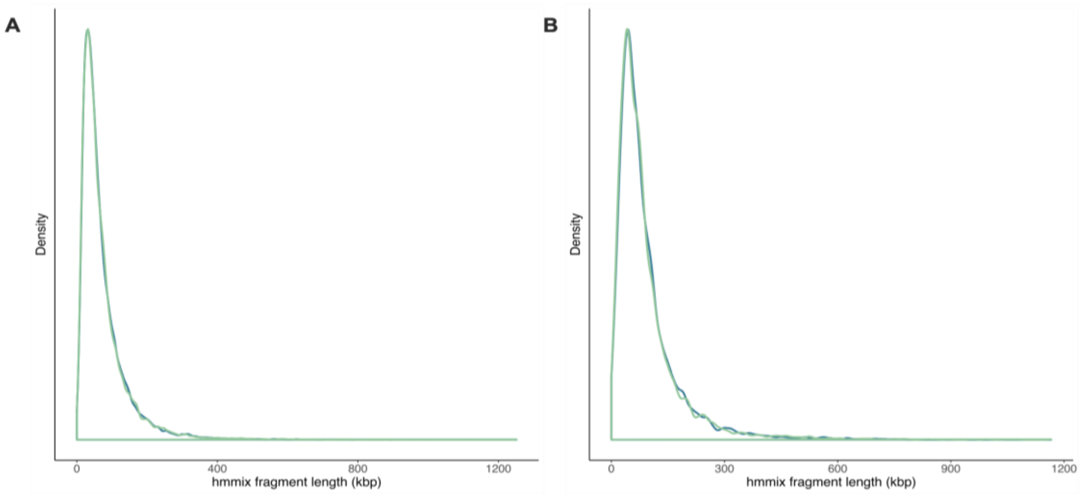

Supplementary Figure 12: Distribution of hmmix fragment lengths for mountain gorillas (blue) and eastern lowland gorillas (green) at a threshold of A 0.9 and B 0.95.

When we compare a PCA of putative introgressed regions against a PCA of random regions of equivalent length distribution, we see in the introgressed regions that PCs 1 and 2 explain a greater percentage of the variance (Supplementary Fig. 13). For introgressed regions PC1 exhibits increased separation of eastern from western gorillas, as expected under archaic introgression specifically into eastern gorillas (Kuhlwilm et al., 2019). While PC2 separates out the eastern subspecies to a greater extent than in random regions. We note that in PC1 the target individual carrying the introgressed material tends to fall outside the variation of its subspecies, but this is not always the case, indicative of the population frequency of the introgressed regions. Likewise in phylogenetic trees the target individual carrying the introgressed material has a longer branch, rather than falling basal to the other sequences (Supplementary Fig 14). Haplotype networks of putatively introgressed regions often show expected patterns (Supplementary Fig. 15), where the putatively introgressed haplotype shows an unusually large divergence to the variation observed among gorillas. Among the 20 longest introgressed regions, 90% of the resulting haplotype networks look archaic in origin.

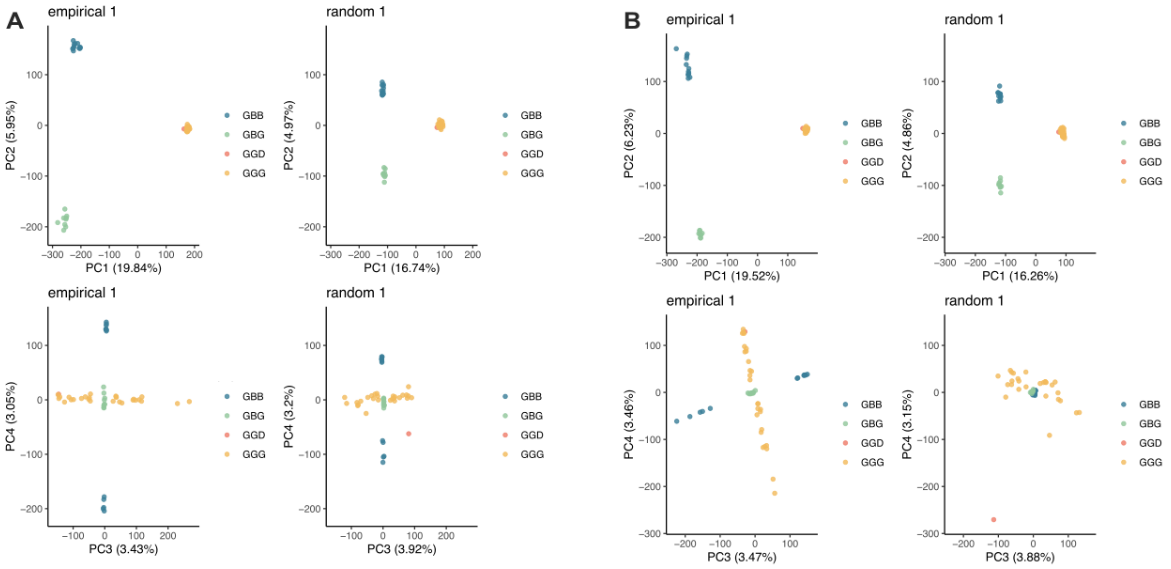

Supplementary Figure 13: A PCA of SNPs in the putative introgressed regions of eastern lowland individual 1 (*Gorilla_beringei_graueri-9732_Mkubwa)* and of random genomic regions of equivalent length distribution. PCs 1-4 are shown. **B** Equivalent PCA analysis for putative introgressed regions of mountain gorilla individual 1 (*Gorilla_beringei_beringei-Bwiruka).*

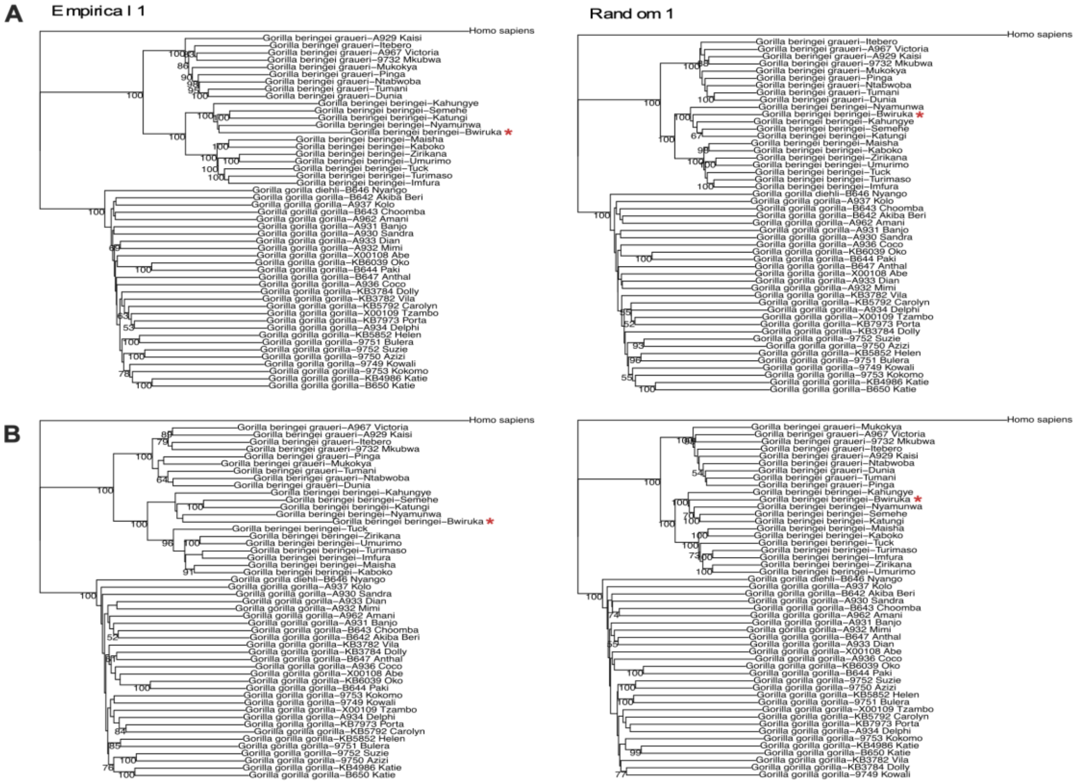
A
Empirica l 1
Homo sapiens
Gorilla beringei graueri–A929 Kaisi
Gorilla beringei graueri–Itebero
Gorilla beringei graueri–A967 Victoria
Gorilla beringei graueri–9732 Mkubwa
Gorilla beringei graueri–Mukokya
Gorilla beringei graueri–Pinga
Gorilla beringei graueri–Ntabwoba
Gorilla beringei graueri–Tumani
Gorilla beringei graueri–Dunia
Gorilla beringei beringei–Kahungye
Gorilla beringei beringei–Semehe
Gorilla beringei beringei–Katungi
Gorilla beringei beringei–Nyamunwa
Gorilla beringei beringei–Bwiruka *
Gorilla beringei beringei–Maisha
Gorilla beringei beringei–Kaboko
Gorilla beringei beringei–Zirikana
Gorilla beringei beringei–Umurimo
Gorilla beringei beringei–Tuck
Gorilla beringei beringei–Turimaso
Gorilla beringei beringei–Imfura
Gorilla gorilla diehli–B646 Nyango
Gorilla gorilla gorilla–B642 Akiba Beri
Gorilla gorilla gorilla–A937 Kolo
Gorilla gorilla gorilla–B643 Choomba
Gorilla gorilla gorilla–A962 Amani
Gorilla gorilla gorilla–A931 Banjo
Gorilla gorilla gorilla–A930 Sandra
Gorilla gorilla gorilla–A933 Dian
Gorilla gorilla gorilla–A932 Mimi
Gorilla gorilla gorilla–X00108 Abe
Gorilla gorilla gorilla–KB6039 Oko
Gorilla gorilla gorilla–B644 Paki
Gorilla gorilla gorilla–B647 Anthal
Gorilla gorilla gorilla–A936 Coco
Gorilla gorilla gorilla–KB3784 Dolly
Gorilla gorilla gorilla–KB3782 Vila
Gorilla gorilla gorilla–KB5792 Carolyn
Gorilla gorilla gorilla–X00109 Tzambo
Gorilla gorilla gorilla–KB7973 Porta
Gorilla gorilla gorilla–A934 Delphi
Gorilla gorilla gorilla–KB5852 Helen
Gorilla gorilla gorilla–9751 Bulera
Gorilla gorilla gorilla–9752 Suzie
Gorilla gorilla gorilla–9750 Azizi
Gorilla gorilla gorilla–9749 Kowali
Gorilla gorilla gorilla–9753 Kokomo
Gorilla gorilla gorilla–KB4986 Katie
Gorilla gorilla gorilla–B650 Katie
Rand om 1
Homo sapiens
Gorilla beringei graueri–Itebero
Gorilla beringei graueri–A967 Victoria
Gorilla beringei graueri–A929 Kaisi
Gorilla beringei graueri–9732 Mkubwa
Gorilla beringei graueri–Mukokya
Gorilla beringei graueri–Pinga
Gorilla beringei graueri–Ntabwoba
Gorilla beringei graueri–Tumani
Gorilla beringei graueri–Dunia
Gorilla beringei beringei–Nyamunwa
Gorilla beringei beringei–Bwiruka *
Gorilla beringei beringei–Kahungye
Gorilla beringei beringei–Semehe
Gorilla beringei beringei–Katungi
Gorilla beringei beringei–Maisha
Gorilla beringei beringei–Kaboko
Gorilla beringei beringei–Zirikana
Gorilla beringei beringei–Umurimo
Gorilla beringei beringei–Tuck
Gorilla beringei beringei–Turimaso
Gorilla beringei beringei–Imfura
Gorilla gorilla diehli–B646 Nyango
Gorilla gorilla gorilla–A937 Kolo
Gorilla gorilla gorilla–B643 Choomba
Gorilla gorilla gorilla–B642 Akiba Beri
Gorilla gorilla gorilla–A962 Amani
Gorilla gorilla gorilla–A931 Banjo
Gorilla gorilla gorilla–A930 Sandra
Gorilla gorilla gorilla–A936 Coco
Gorilla gorilla gorilla–KB6039 Oko
Gorilla gorilla gorilla–B644 Paki
Gorilla gorilla gorilla–B647 Anthal
Gorilla gorilla gorilla–X00108 Abe
Gorilla gorilla gorilla–A933 Dian
Gorilla gorilla gorilla–A932 Mimi
Gorilla gorilla gorilla–KB3782 Vila
Gorilla gorilla gorilla–KB5792 Carolyn
Gorilla gorilla gorilla–A934 Delphi
Gorilla gorilla gorilla–X00109 Tzambo
Gorilla gorilla gorilla–KB7973 Porta
Gorilla gorilla gorilla–KB3784 Dolly
Gorilla gorilla gorilla–9752 Suzie
Gorilla gorilla gorilla–9750 Azizi
Gorilla gorilla gorilla–KB5852 Helen
Gorilla gorilla gorilla–9751 Bulera
Gorilla gorilla gorilla–9749 Kowali
Gorilla gorilla gorilla–9753 Kokomo
Gorilla gorilla gorilla–KB4986 Katie
Gorilla gorilla gorilla–B650 Katie
B
Homo sapiens
Gorilla beringei graueri–A967 Victoria
Gorilla beringei graueri–A929 Kaisi
Gorilla beringei graueri–Itebero
Gorilla beringei graueri–9732 Mkubwa
Gorilla beringei graueri–Pinga
Gorilla beringei graueri–Mukokya
Gorilla beringei graueri–Tumani
Gorilla beringei graueri–Ntabwoba
Gorilla beringei graueri–Dunia
Gorilla beringei beringei–Kahungye
Gorilla beringei beringei–Semehe
Gorilla beringei beringei–Katungi
Gorilla beringei beringei–Nyamunwa
Gorilla beringei beringei–Bwiruka *
Gorilla beringei beringei–Tuck
Gorilla beringei beringei–Zirikana
Gorilla beringei beringei–Umurimo
Gorilla beringei beringei–Turimaso
Gorilla beringei beringei–Imfura
Gorilla beringei beringei–Maisha
Gorilla beringei beringei–Kaboko
Gorilla gorilla diehli–B646 Nyango
Gorilla gorilla gorilla–A937 Kolo
Gorilla gorilla gorilla–A930 Sandra
Gorilla gorilla gorilla–A933 Dian
Gorilla gorilla gorilla–A932 Mimi
Gorilla gorilla gorilla–A962 Amani
Gorilla gorilla gorilla–A931 Banjo
Gorilla gorilla gorilla–B643 Choomba
Gorilla gorilla gorilla–B642 Akiba Beri
Gorilla gorilla gorilla–KB3782 Vila
Gorilla gorilla gorilla–KB3784 Dolly
Gorilla gorilla gorilla–B647 Anthal
Gorilla gorilla gorilla–A936 Coco
Gorilla gorilla gorilla–X00108 Abe
Gorilla gorilla gorilla–KB6039 Oko
Gorilla gorilla gorilla–B644 Paki
Gorilla gorilla gorilla–9753 Kokomo
Gorilla gorilla gorilla–9749 Kowali
Gorilla gorilla gorilla–X00109 Tzambo
Gorilla gorilla gorilla–A934 Delphi
Gorilla gorilla gorilla–KB7973 Porta
Gorilla gorilla gorilla–KB5792 Carolyn
Gorilla gorilla gorilla–KB5852 Helen
Gorilla gorilla gorilla–9751 Bulera
Gorilla gorilla gorilla–9752 Suzie
Gorilla gorilla gorilla–9750 Azizi
Gorilla gorilla gorilla–KB4986 Katie
Gorilla gorilla gorilla–B650 Katie
Homo sapiens
Gorilla beringei graueri–Mukokya
Gorilla beringei graueri–A967 Victoria
Gorilla beringei graueri–9732 Mkubwa
Gorilla beringei graueri–Itebero
Gorilla beringei graueri–A929 Kaisi
Gorilla beringei graueri–Ntabwoba
Gorilla beringei graueri–Dunia
Gorilla beringei graueri–Tumani
Gorilla beringei graueri–Pinga
Gorilla beringei beringei–Kahungye
Gorilla beringei beringei–Bwiruka *
Gorilla beringei beringei–Nyamunwa
Gorilla beringei beringei–Semehe
Gorilla beringei beringei–Katungi
Gorilla beringei beringei–Maisha
Gorilla beringei beringei–Kaboko
Gorilla beringei beringei–Tuck
Gorilla beringei beringei–Turimaso
Gorilla beringei beringei–Imfura
Gorilla beringei beringei–Zirikana
Gorilla beringei beringei–Umurimo
Gorilla gorilla diehli–B646 Nyango
Gorilla gorilla gorilla–A937 Kolo
Gorilla gorilla gorilla–B642 Akiba Beri
Gorilla gorilla gorilla–A930 Sandra
Gorilla gorilla gorilla–B643 Choomba
Gorilla gorilla gorilla–A962 Amani
Gorilla gorilla gorilla–A931 Banjo
Gorilla gorilla gorilla–A932 Mimi
Gorilla gorilla gorilla–B647 Anthal
Gorilla gorilla gorilla–A933 Dian
Gorilla gorilla gorilla–X00108 Abe
Gorilla gorilla gorilla–A936 Coco
Gorilla gorilla gorilla–KB6039 Oko
Gorilla gorilla gorilla–B644 Paki
Gorilla gorilla gorilla–9752 Suzie
Gorilla gorilla gorilla–9750 Azizi
Gorilla gorilla gorilla–KB5852 Helen
Gorilla gorilla gorilla–9751 Bulera
Gorilla gorilla gorilla–X00109 Tzambo
Gorilla gorilla gorilla–KB5792 Carolyn
Gorilla gorilla gorilla–KB7973 Porta
Gorilla gorilla gorilla–A934 Delphi
Gorilla gorilla gorilla–9753 Kokomo
Gorilla gorilla gorilla–KB4986 Katie
Gorilla gorilla gorilla–B650 Katie
Gorilla gorilla gorilla–KB3782 Vila
Gorilla gorilla gorilla–KB3784 Dolly
Gorilla gorilla gorilla–9749 Kowali

Supplementary Figure 14: A NJ tree of SNPs in all putative introgressed regions of mountain gorilla individual 1 (*Gorilla_beringei_beringei-Bwiruka)* and of random genomic regions of equivalent length distribution. **B** NJ tree of SNPs in putative introgressed regions unique to mountain gorilla individual 1 (so-called ‘private introgressed regions’) and equivalent random genomic regions. The target individual is indicated by a red star.

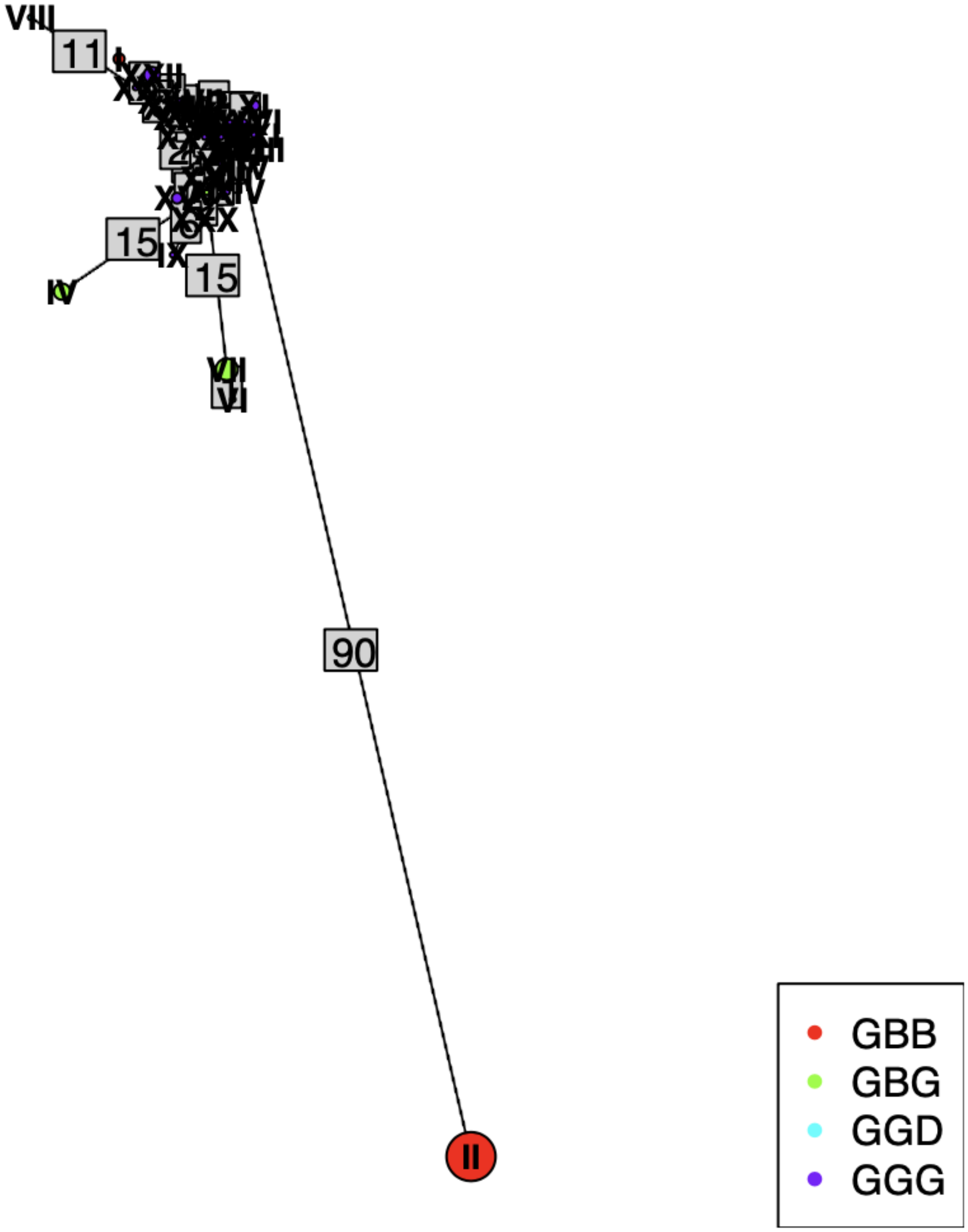

Supplementary Figure 15: Haplotype network of one of the putative introgressed regions (chr13: 79839000-80119000), which looks characteristic of archaic introgression, where haplotype II carried by mountain gorillas is far outside the diversity of other gorillas.

4.2 Introgression and selection

We find no depletion in the proportion of protein-coding base pairs (bp) in the introgressed regions compared to random regions of the genome (Supplementary Fig. 16). Putative deserts of introgression of more than 5 Mbp are rare (Supplementary Fig. 17). In Supplementary Fig. 18, we show the likelihood scores for candidate genes for adaptive introgression, using VolcanoFinder.

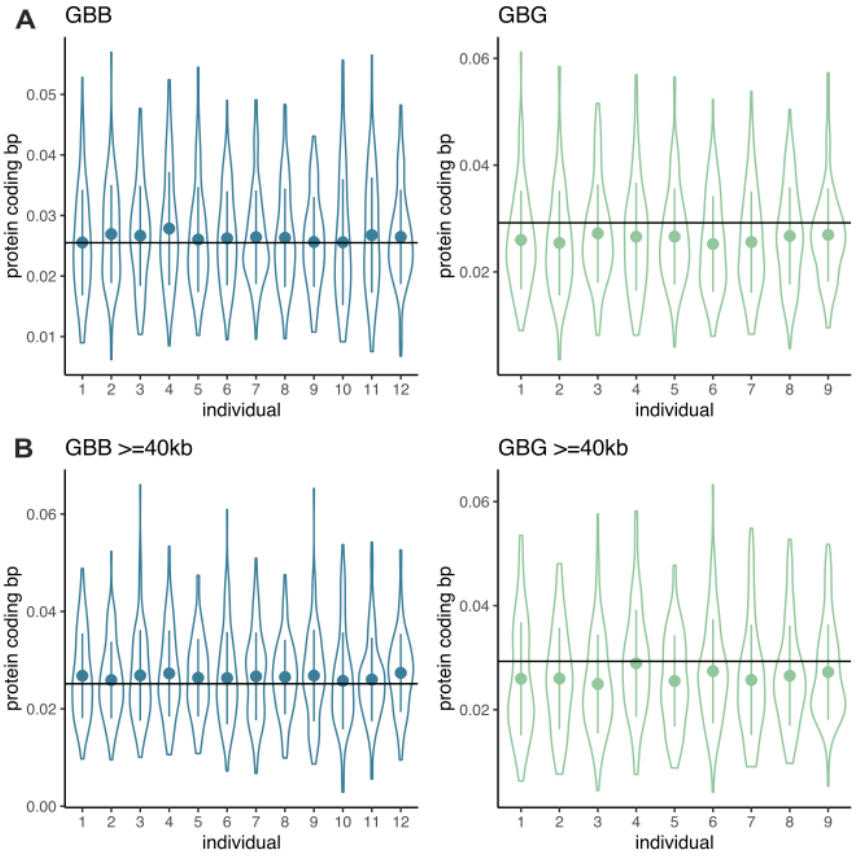

Supplementary Figure 16: A Proportion of protein coding base pairs in putative introgressed regions (lines) and in random genomic regions (violin plots) per individual for both eastern gorilla populations. **B** Proportion of protein coding base pairs in putative introgressed regions of length >= 40kb (lines) and in equivalent random genomic regions (violin plots) per individual. Data for n=100 iterations of random genomic regions are presented in violin plots with means +/- standard deviation.

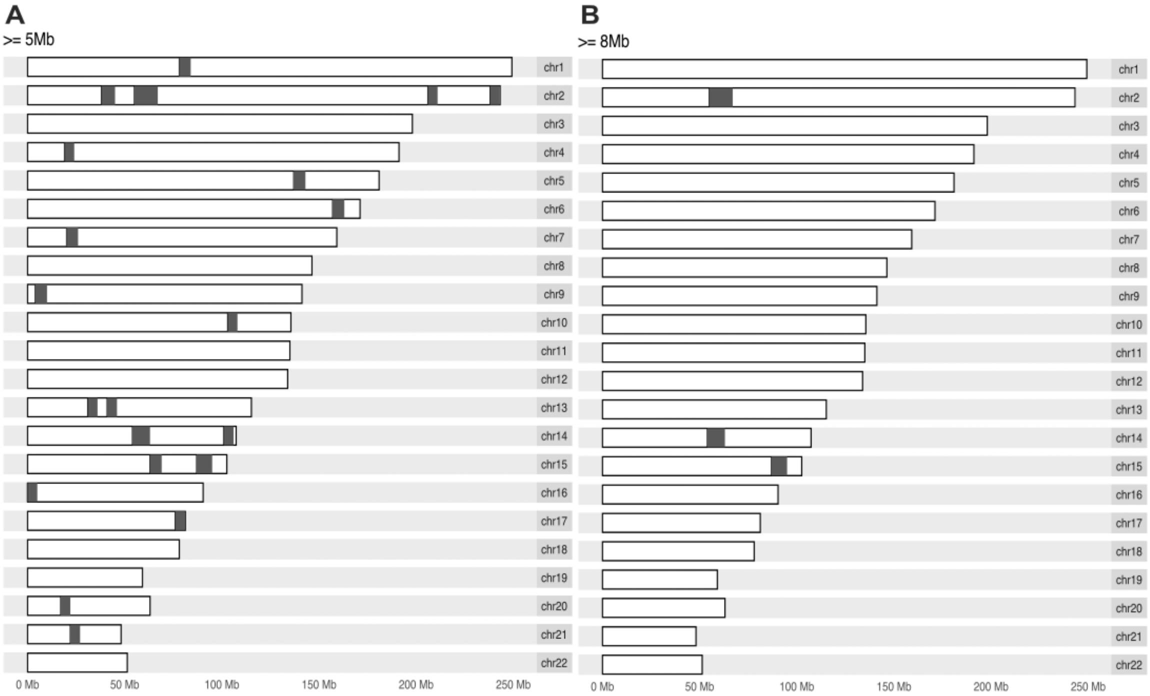

Supplementary Figure 17: Distribution of regions depleted of archaic introgression **A** regions of length >=5Mb **B** regions of length >=8Mb.

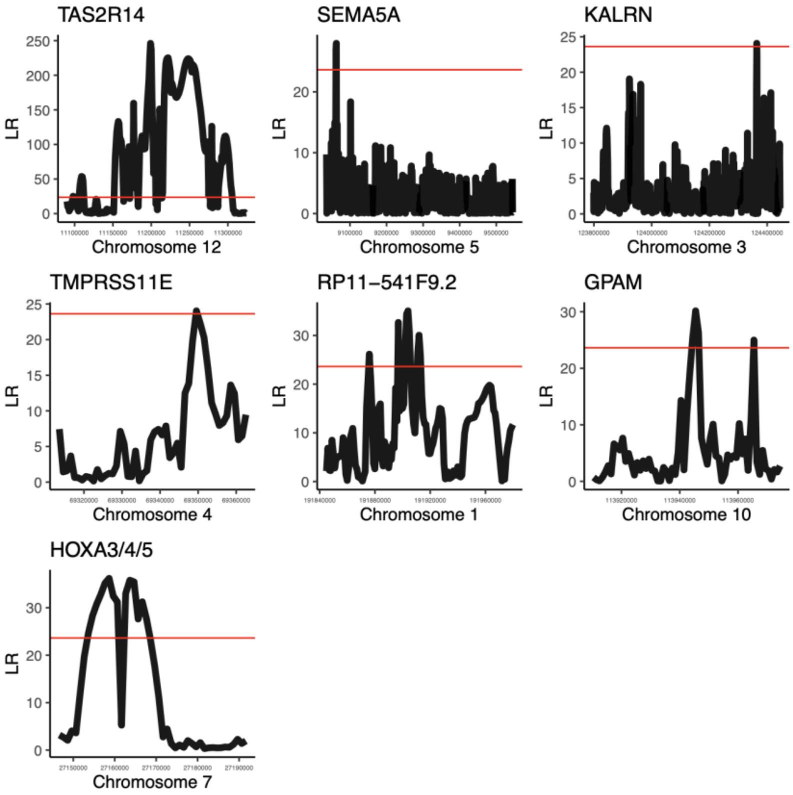

Supplementary Figure 18: Likelihood ratio scores for the seven candidate genes of adaptive introgression, estimated with VolcanoFinder. Red line indicates the 95% threshold for the VolcanoFinder likelihood ratio score.

4.3 Functional consequences: mutational tolerance

To address the question of mutational tolerance, specifically whether more deleterious mutations are observed in introgressed rather than random genomic regions, we assessed different measures of deleteriousness, using: genomic evolutionary rate profiling (GERP), sorting intolerant from tolerant (SIFT), polymorphism phenotyping (PolyPhen-2) and LINSIGHT scores [58,59,60,61]. We downloaded the pre-computed base-wise GERP scores for hg19[58] and considered sites (>4) as having high functional impact and sites (-2<x<2) as having low or likely neutral impact. SIFT and PolyPhen-2 scores were extracted from VEP annotation for missense variants. We consider sites annotated with (SIFT=‘deleterious’ or ‘deleterious_low_confidence’; PolyPhen-2=‘probably_damaging’ or ‘possibly_damaging’) as high impact and (SIFT=‘tolerated’ or ‘tolerated_low_confidence’; PolyPhen-2=’benign’) as low impact. LINSIGHT scores incorporate epigenomic information, including chromatin accessibility and transcription factor binding[61]. We downloaded the pre-calculated LINSIGHT scores for hg19[61].

For GERP, SIFT and PolyPhen-2 scores we calculated the proportion of high impact sites within putative introgressed regions and random regions of equal length distribution and sufficient callable sites (high / high and low impact sites). We calculated the mean LINSIGHT score across regions, since few high impact sites (>0.8) were identified in our dataset. We find a higher proportion of high impact GERP sites in introgressed regions of eastern lowland gorillas compared to mountain gorillas (Fig. 3E). However, for SIFT, PolyPhen-2 and LINSIGHT scores the introgressed regions of both eastern lowland and mountain gorillas follow random expectation (Supplementary Fig. 19).

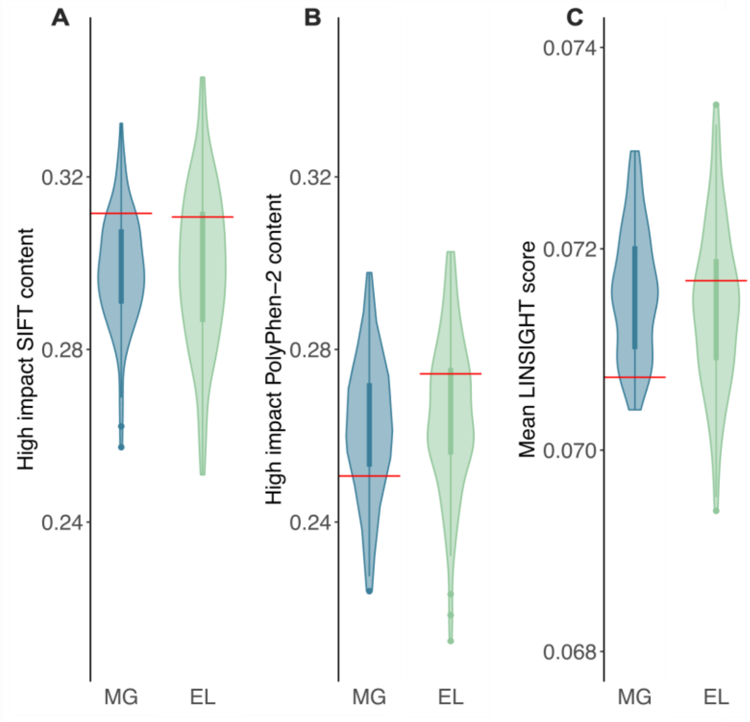

Supplementary Figure 19: Mutational conservation in introgressed fragments. Proportion of high impact sites in introgressed regions (red lines) and random regions (violin plots) for **A** SIFT scores and **B** PolyPhen-2 scores. High impact sites are those annotated as 'deleterious' and 'deleterious low confidence' for SIFT, and 'probably damaging' and 'possibly damaging' for PolyPhen-2. **C** Mean LINSIGHT score across introgressed regions (red lines) and random regions (violin plots). In panels A-C MG = mountain gorillas, EL = eastern lowlands. Data for n=100 iterations of random genomic regions are presented in violin plots with overlaid boxplots, which represent the median and interquartile range (25th and 75th percentiles).

4.4 Functional consequences: regulatory elements

We undertook an investigation of regulatory elements in introgressed fragments. We assessed the proportion of regulatory base pairs within putative introgressed and random regions of equivalent length and callability, using the gorilla-defined regulatory element annotations of García-Pérez et al.[34]. We assess this both from a global perspective and per regulatory element type (poised, strong, weak, enhancers and promoters). To do this, we performed a sequential liftover of the coordinates from gorGor4 to hg38 to hg19, to match the genomic coordinates used for the rest of our analyses. We filtered out entries corresponding to non-regulatory elements in at least one of the two replicates of gorilla lymphoblastoid cells (Non-re, E/Non-re and P/Non-re). We also filtered out entries annotated as ambiguous (aE, aP, P/E).

We note that this data derives from gorilla lymphoblastoid cells (LCLs), which means that the patterns of expression may be cell-type dependent and specific regulatory effects, for example during brain development, would not be recovered. This is an inherent limitation of this kind of analysis in a non-human context. Moreover, the two gorilla LCL replicates belonged to the western species, hence are equidistant to both eastern subspecies.

We assessed the gene regulatory architecture of strong enhancers (sE) in mountain gorilla introgressed regions and equivalent random genomic regions, using the definitions of García-Pérez et al.[34]. We considered enhancer-interacting enhancers, intragenic enhancers, enhancers within promoters (genic promoters), promoter-interacting enhancers and proximal enhancers (EiE, gE, gP, PiE, prE). This analysis is restricted to sE associated with genes.

We find no difference in the overall proportion of regulatory base pairs in putative introgressed regions compared to random genomic regions for either eastern gorilla population (Supplementary Fig. 20A). However, when we consider the proportion of regulatory base pairs per regulatory element we see an excess of sE in mountain gorilla introgressed regions, compared to random regions (Supplementary Fig. 20B). These sE are largely intragenic enhancers (Supplementary Fig. 21), which agrees with patterns of regulatory architecture observed in primate sE more generally by [34].

Furthermore, García-Pérez et al.[34] had annotated which genes are associated with each regulatory element. Taking these annotations and filtering to genes with one-to-one orthologs across the primates considered by García-Pérez et al.[34] (humans, chimpanzees, gorillas, orangutans and macaques) we define two sets of candidate genes: 1) genes regulated by sE in mountain gorilla introgressed regions (235 genes), and 2) genes regulated by sE in mountain gorilla adaptively introgressed regions (45 genes) (Supplementary Tables 16-17). We performed an over-representation analysis of our candidate genes for gene ontology terms using the WebGestaltR package and default settings[77]. Our background set consisted of genes regulated by gorilla sE (again taking those genes with one-to-one orthologs in primates) (Supplementary Table 18). No gene ontology category reached the significance threshold of FDR=0.05 with Benjamini-Hochberg correction (Supplementary Fig. 22). The top gene ontology categories detected relate to the LCL cell type, namely ‘establishment of lymphocyte polarity’ (p-value=0.00018256, FDR=0.38985) and ‘establishment of T cell polarity’ (p-value=0.00018256, FDR=0.38985) for candidate gene set 1) and ‘forebrain generation of neurons’ (p-value=0.000066791, FDR=0.14263) for candidate gene set 2).

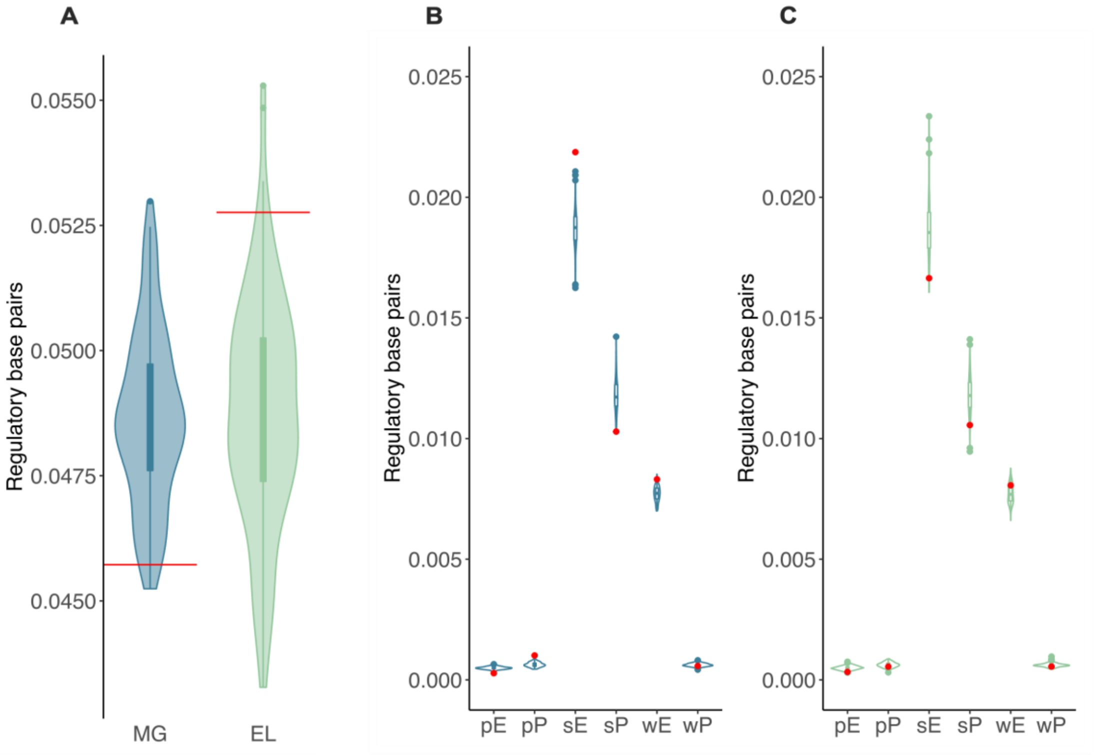

Supplementary Figure 20: Proportion of regulatory base pairs in introgressed regions (red lines) and random regions (violin plots) population wide in **A** and per regulatory element type for **B** mountain gorillas and **C** eastern lowland gorillas. Abbreviations represent: pE=poised enhancer, pP=poised promoter, sE=strong enhancer, sP=strong promoter, wE=weak enhancer, wP=weak promoter. In panel A MG = mountain gorillas, EL = eastern lowlands. Data for n=100 iterations of random genomic regions are presented in violin plots with overlaid boxplots, which represent the median and interquartile range (25th and 75th percentiles).

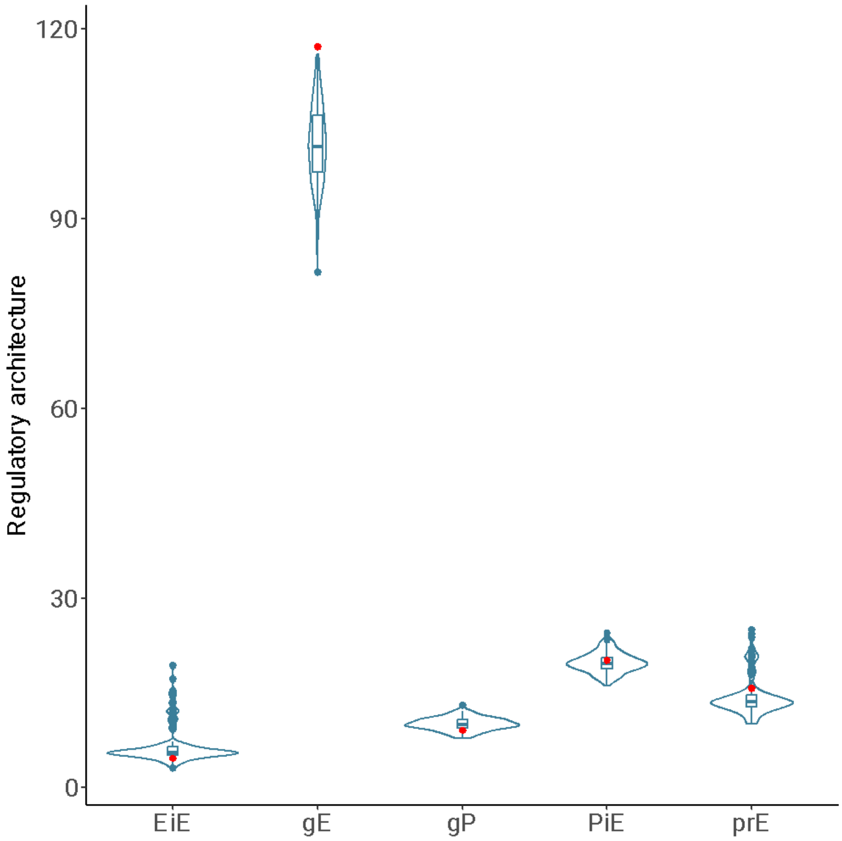

Supplementary Figure 21: Gene regulatory architecture of strong enhancers in mountain gorilla introgressed regions (red points) and random genomic regions of equivalent length and callability (violin plots). Abbreviations represent: EiE=enhancer-interacting enhancer, gE=intragenic enhancer, gP=genic promoter, PiE=promoter-interacting enhancer, prE=proximal enhancer. This analysis only considers those strong enhancers which could be annotated to genes by [34]. Data for n=100 iterations of random genomic regions are presented in violin plots with overlaid boxplots, which represent the median and interquartile range (25th and 75th percentiles).

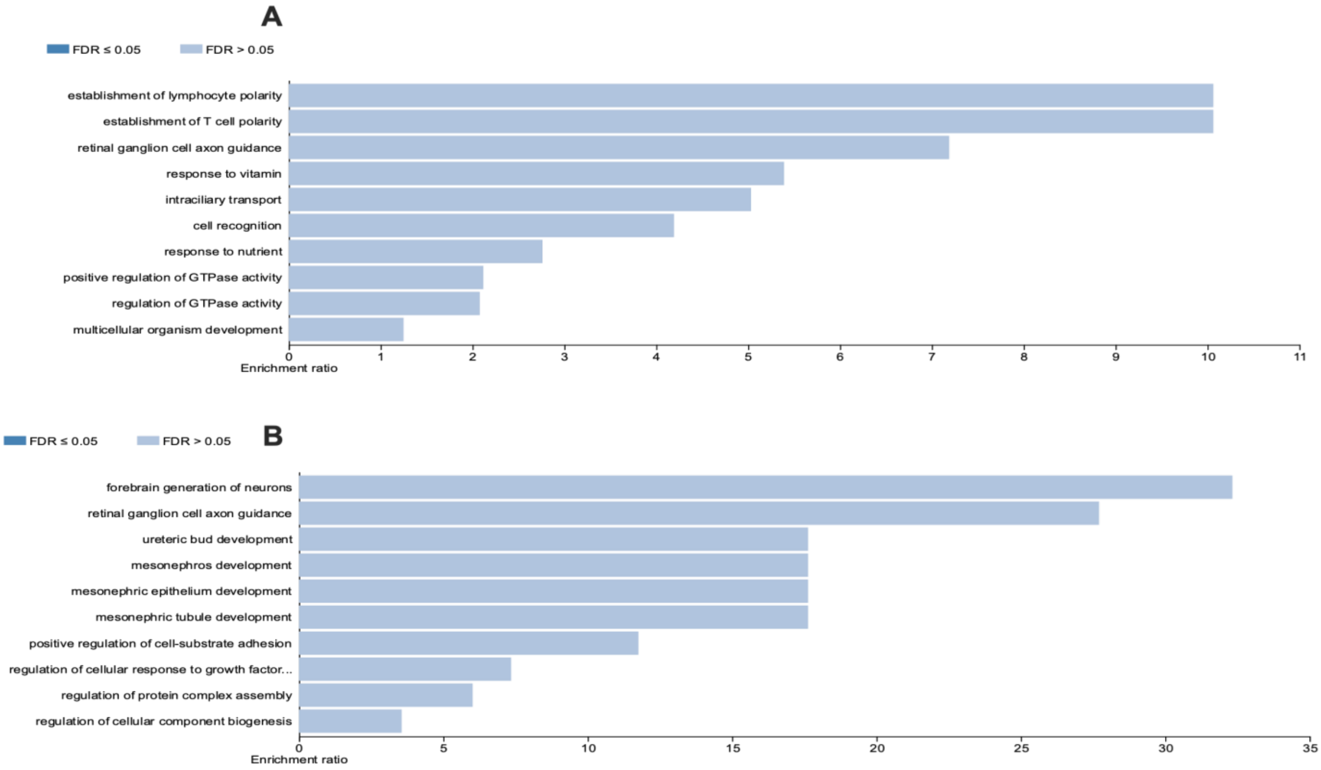

Supplementary Figure 22: Over-representation in gene ontology categories for **A** genes regulated by sE in mountain gorilla introgressed regions and **B** genes regulated by sE in mountain gorilla adaptively introgressed regions. No category reaches significance at FDR=0.05 with Benjamini-Hochberg correction.

Supplementary References

71. Maier, Robert, Pavel Flegontov, Olga Flegontova, Ulas Isildak, Piya Changmai, and David Reich. 2023. On the Limits of Fitting Complex Models of Population History to - Statistics. *eLife* 12: e85492. https://doi.org/10.7554/eLife.85492.
72. Sorensen, Erik F., R. Alan Harris, Liye Zhang, Muthuswamy Raveendran, Lukas F. K. Kuderna, Jerilyn A. Walker, Jessica M. Storer, et al. 2023, “Genome-wide coancestry reveals details of ancient and recent male-driven reticulation in baboons.” *Science* (in press).
73. Wegmann, Daniel, Christoph Leuenberger, and Laurent Excoffier. 2009. “Efficient Approximate Bayesian Computation Coupled with Markov Chain Monte Carlo without Likelihood.” *Genetics* 182 (4): 1207–18.
74. Wegmann, Daniel, Christoph Leuenberger, Samuel Neuenschwander, and Laurent Excoffier. 2010. “ABCtoolbox: A Versatile Toolkit for Approximate Bayesian Computations.” *BMC Bioinformatics* 11 (1): 116.
75. Luqman, Hirzi, Alex Widmer, Simone Fior, and Daniel Wegmann. 2021. “Identifying Loci under Selection via Explicit Demographic Models.” *Molecular Ecology Resources* 21 (8): 2719–37.
76. Gower, Graham, Aaron P. Ragsdale, Gertjan Bisschop, Ryan N. Gutenkunst, Matthew Hartfield, Ekaterina Noskova, Stephan Schiffels, Travis J. Struck, Jerome Kelleher, and Kevin R. Thornton. 2022. “Demes: A Standard Format for Demographic Models.” *Genetics* 222 (3): iyac131. https://doi.org/10.1093/genetics/iyac131.
77. Liao, Y., Wang, J., Jaehnig, E. J., Shi, Z. & Zhang, B. WebGestalt 2019. gene set analysis toolkit with revamped UIs and APIs. *Nucleic Acids Res.* 47, W199–W205.